Article

Base-Free Aerobic Oxidation of 5-Hydroxymethylfurfural to 2,5-Furandicarboxylic Acid in Water Catalyzed by Functionalized Carbon Nanotube-Supported Au-Pd Alloy Nanoparticles

Xiaoyue Wan, Chunmei Zhou, Jiashu Chen, Weiping Deng, Qinghong Zhang, Yanhui Yang, and Ye Wang

ACS Catal., **Just Accepted Manuscript** • DOI: 10.1021/cs5003096 • Publication Date (Web): 26 May 2014

Base-Free Aerobic Oxidation of 5-Hydroxymethyl-furfural to 2,5-Furandicarboxylic Acid in Water Catalyzed by Functionalized Carbon Nanotube-Supported Au-Pd Alloy Nanoparticles

Xiaoyue Wan,[†] Chunmei Zhou,[‡] Jiashu Chen,[†] Weiping Deng,[†] Qinghong Zhang,[†] Yanhui Yang,[‡] and Ye Wang*[†]*

[†]State Key Laboratory of Physical Chemistry of Solid Surfaces, Collaborative Innovation Center of Chemistry for Energy Materials, National Engineering Laboratory for Green Chemical Productions of Alcohols, Ethers and Esters, College of Chemistry and Chemical Engineering, Xiamen University, Xiamen 361005, China

[‡]School of Chemical and Biomedical Engineering, Nanyang Technological University, Singapore 637459, Singapore

***CORRESPONDING AUTHOR: **E-mail:** wangye@xmu.edu.cn or zhanqh@xmu.edu.cn; **Phone:** +86-592-2186156; **Fax:** +86-592-2183047

ABSTRACT: The aerobic oxidation of 5-hydroxymethylfurfural (HMF), a key platform compound in cellulose transformation, into 2,5-furandicarboxylic acid (FDCA), a promising renewable alternative to petroleum-derived terephthalic acid, is one of the most attractive reactions for establishing the biomass-based sustainable chemical processes. Supported Au catalysts have shown encouraging performance for this reaction, but the need of excess amount of base additives makes the process less green and less cost-effective. Here, we report an efficient and stable carbon nanotube (CNT)-supported Au-Pd alloy catalyst for the aerobic oxidation of HMF to FDCA in water without any bases. The functionalization of CNT surfaces is crucial for FDCA formation. We have clarified that the CNT containing more carbonyl/quinone and less carboxyl groups favors FDCA formation by enhancing the adsorption of the reactant and reaction intermediates. Significant synergistic effects exist between Au and Pd in the alloy for the base-free oxidation of HMF to FDCA through three tandem steps. The present work provides deep understanding of the support-enhanced adsorption effect and the alloying effect for supported Au-based bimetallic catalysts, and may help develop efficient catalysts for the aerobic oxidation of relatively complicated organic compounds with different functional groups in water.

KEYWORDS: aerobic oxidation, 5-hydroxymethylfurfural, sustainable chemistry, carbon nanotube, gold catalysis, alloying effect

1. INTRODUCTION

The depletion of fossil resources has stimulated recent research activities for the utilization of renewable biomass resources for the sustainable production of chemicals. An ideal route for the chemical utilization of cellulose, which is the main component of the abundant and non-edible lignocellulosic biomass, is to develop catalytic processes for the selective conversion of cellulose into a platform compound under mild conditions, followed by subsequent production of high-valued chemicals from the platform compound.[1-7] 5-Hydroxymethylfurfural (HMF) is a promising platform compound from cellulose or cellulose-derived carbohydrates.[8-13] The aerobic oxidation of HMF into 2,5-furandicarboxylic acid (FDCA) (Equation (1)) is one of the most attractive reactions for establishing biomass-based sustainable chemical processes via HMF, since FDCA is a versatile building-block chemical.[14] In particular, FDCA is a promising renewable alternative to terephthalic acid, which is a petroleum-derived monomer and is widely used for the production of key polymers such as polyethylene terephthalate (PET) and polybutyleneterephthalate (PBT) plastics.[14,15]

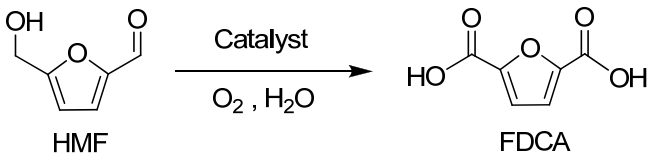

Equation (1)

On the other hand, gold catalysis has attracted much attention in recent years.[16-19] In addition to the well-known examples for CO oxidation and propylene epoxidation,[20-24] supported Au catalysts can catalyze the aerobic oxidation of various substrates in the liquid phase.[25-29] It is generally accepted that the Au-based catalysts are more stable and selective for the aerobic oxidation of organic compounds in water than the conventional liquid-phase oxidation catalysts based on Pt and Pd because the Au catalysts can offer better resistance to water and O_2.[18,25-29] However, Au may be deactivated more easily by the formed organic products or intermediates

such as carboxylic acid in the absence of a base promoter.[30] The alloying of another metal (e.g., Pd and Pt) with Au to form bimetallic alloy catalysts may combine the advantages (functions) of different components in atomic level and may enhance the activity and stability. Such an alloying effect has been found in many aerobic oxidation reactions.[30-41] In particular, Hutchings and co-workers have demonstrated that the supported Au-Pd alloy catalysts show excellent performances for many oxidation reactions such as the direct synthesis of H_2O_2 and the selective oxidation of alcohols or hydrocarbons.[31,34-41] Many useful insights have been obtained from these systems, nevertheless, more knowledge on the deep understanding of the alloying effect is still needed.

The aerobic oxidation of HMF to FDCA requires the oxidation of both the hydroxyl and the aldehyde groups to carboxyl groups (Equation (1)). The formation of FDCA is expected to involve several tandem oxidation steps. Thus, the catalyst design for the aerobic oxidation of HMF to FDCA is more complicated than that for simpler oxidation reactions such as the oxidation of alcohols or aldehydes. Supported Au nanoparticles have shown encouraging catalytic performances for the aerobic oxidation of HMF to FDCA in water,[42-47] although Pt-, Pd-, or Ru-based catalysts can also catalyze the selective oxidation of HMF to FDCA or 2,5-diformylfuran (DFF).[48-53] However, the stability of the supported Au catalysts in the aerobic oxidation of HMF remains a problem. Another serious problem is the requirement of excess amount of a base additive such as NaOH. The neutralization of the salt of carboxylic acid product would further increase the operating cost and produce additional salt byproducts, making the process less green and less cost-effective. The employment of methanol as a solvent instead of water to produce dimethylfuroate may avoid the use of bases, but the oxidation of methanol

also occurs under the reaction conditions.[54-56] The use of methanol as a solvent in the presence of O_2 may cause explosion problem in practical large-scale production.

Thus far, only Au loaded on hydrotalcite (HT), a strong solid base, has been claimed to catalyze the aerobic oxidation of HMF to FDCA in water without a liquid base.[44,46] However, extensive leaching of magnesium from HT due to the chemical interaction between the basic HT and the formed FDCA occurred inevitably.[46] Therefore, the development of stable heterogeneous catalysts for the aerobic oxidation of HMF under base-free conditions remains challenging.

Generally, the supported Au catalysts are less efficient for the oxidation of alcohol than that of aldehyde.[26] Au catalysts are almost inert for the aerobic oxidation of alcohol in the absence of base additives or basic supports.[57] Actually, the oxidation of the hydroxyl group in HMF has been reported to proceed slower than that of the aldehyde group over the Au-based catalysts even with a base additive.[42-47] A few bimetallic catalysts such as supported Au-Cu and Au-Pd alloys have been reported to be more efficient and stable than the monometallic Au catalysts.[58,59] However, the nature of the alloying effect is still unclear. Furthermore, the base promoters have still been employed in these systems.

Recently, we have attempted to develop stable heterogeneous catalysts for the base-free aerobic oxidation of HMF to FDCA. Considering that the Au-Pd alloy can catalyze the oxidation of alcohols very efficiently,[30,31] we have studied systematically the catalytic behaviors of the Au-Pd nanoparticles loaded on various supports for the aerobic oxidation of HMF in water in the absence of any bases. This article reports for the first time an efficient and recyclable carbon nanotube (CNT)-supported Au-Pd alloy catalyst for the base-free aerobic oxidation of HMF to FDCA. The roles of the CNT, particularly the functional groups on CNT surfaces, will be discussed in detail. We will show how the catalyst support can play roles in the liquid-phase

aerobic oxidation of organic molecules in water, which is a kind of very important green chemical reactions, by enhancing the adsorption of the reactant and intermediates. We will also demonstrate how the cooperative effect between Au and Pd in the alloy contributes to realizing the base-free production of FDCA from HMF.

2. EXPERIMENTAL SECTION

2.1. Materials. The supports employed in the work included oxides (including SiO_2, Al_2O_3, TiO_2, ZrO_2, CeO_2, and MgO with purities >99% purchased from Sinopharm or Alfa-Aesar), hydrotalcite (HT), and carbon materials. Carbon nanofibers (CNFs) were purchased from Winchem Industrial Co. Ltd. Multiwalled CNTs with outer diameters of 20-60 nm and inner diameters of 3-5 nm were synthesized by a method reported previously.[60] The CNT and CNF were typically pretreated by 5 wt% HCl at 323 K for 2 h to remove the remaining Ni catalyst used for the synthesis of CNTs or other possible metal impurities. Hydrotalcite (HT) and graphene oxide (GO) were synthesized by the procedures reported previously.[61,62] To study the effect of functional groups on CNTs or CNFs, concentrated HNO_3 and H_2O_2 were also employed to further treat the CNTs or CNFs, which had been pretreated by 5 wt% HCl. The treatments by HNO_3 with concentrations of 30 and 68 wt% were carried out at 413 K under refluxing conditions for 2 h. The treatment with 30 wt% H_2O_2 was performed at 338 K for 6 d. A certain amount of 30 wt% H_2O_2 (4 mL for 0.5 g CNTs or CNFs) was added into the system every 12 h. The powdery CNTs or CNFs after each treatment were recovered by filtration, followed by thorough washing with deionized water and drying at 373 K. In the case of H_2O_2 treatment, the treated CNTs or CNFs underwent further drying at 423 K for 6 h in vacuum to remove the

remaining H_2O_2.[63] The specific surface areas and the structure information of the supports were summarized in Table S1 in the Supporting Information.

Colloidal Au-Pd nanoparticles stabilized with polyvinyl alcohol (PVA) were synthesized by addition of 1.0 wt% PVA (Aldrich, MW = 10000) aqueous solution into a mixed solution of $PdCl_2$ and $HAuCl_4$. The ratio of PVA to (Au + Pd) was controlled at 1.2/1. A freshly prepared $NaBH_4$ solution (0.1 M) was added into the mixture, forming a dark-brown sol containing the colloidal Au-Pd nanoparticles. The molar ratio of $NaBH_4$ to (Au + Pd) was regulated to be 5/1.

The supported Au-Pd bimetallic nanoparticles were prepared by immobilization of the PVA-stabilized colloidal Au-Pd nanoparticles onto different supports. Typically, the powdery support was added into the dark-brown sol with a proper pH under vigorous stirring. When the CNT was used as support, the pH of the sol was adjusted to 7.0 by using diluted HCl aqueous solution. After 2 h, the solid catalyst was recovered by filtration and washed repeatedly with hot distilled water (368 K) to remove the PVA stabilizer.[64] The resultant was dried at 393 K overnight. The supported monometallic catalysts were prepared with the same procedure. The expected loading of metal nanoparticles was typically 1.0 wt% unless otherwise stated.

2.2. Characterizations. Inductively coupled plasma mass spectrometry (ICP-MS) measurements were performed with an Agilent ICP-MS 4500 instrument to measure the actual loadings of Au and Pd in each sample. Specific surface areas of the supports or catalysts were measured by N_2 physisorption with Micromeritics Tristar II 3020. Laser Raman spectroscopic measurements were performed on a Renishaw 1000R Raman system. A green laser at 532 nm was used as the excitation source and the spectra were recorded in the range of 100-2000 cm^{-1}. Transmission electron microscopy (TEM) measurements were performed on a Philips Analytical FEI Tecnai 20 electron microscopy operated at an acceleration voltage of 200 kV. Samples for

TEM measurements were suspended in ethanol and dispersed ultrasonically. Drops of suspensions were applied on a copper grid coated with carbon. X-ray photoelectron spectroscopy (XPS) measurements were performed on a Quantum 2000 Scanning ESCA Microprobe (Physical Electronics) using Al-K_α radiation (1846.6 eV) as the X-ray source. Temperature-programmed desorption (TPD) was carried out using a Micromeritics AutoChem II 2920 instrument. Typically, the sample was loaded and pretreated in a quartz reactor with high-purity Ar (99.999%) at 473 K for 2 h, followed by cooling down to 373 K. Then, the temperature was raised to 1293 K at a rate of 5 K min^{-1}. The desorbed CO and CO_2 were detected with a mass spectrometer (ThermoStar GSD 301 T2) by monitoring the signals with *m/e* = 28 and *m/e* = 44, respectively. The adsorption amounts of the reactant or possible reaction intermediates on various supports or the CNTs pretreated by different methods were measured by addition of the support (0.10 g) into an aqueous solution containing a certain amount of the reactant (HMF) or possible reaction intermediates. The suspension was stirred for 12 h and was allowed to rest for another 12 h at room temperature. The amount of the reactant or possible intermediates remaining in the supernate was measured to determine the adsorption amount.

2.3. Catalytic Reaction. The aerobic oxidation of HMF was performed in a batch-type Teflon-lined stainless-steel autoclave (70 mL). Typically, the powdery catalyst and HMF were added into the reactor pre-charged with H_2O (20 mL). After the purge and the introduction of O_2 with a certain pressure (typically 0.5 MPa), and the reactor was placed in an oil-bath. Once the system reached the desired temperature (typically 373 K), the reaction was initiated by vigorous stirring with a magnet stirrer. The stirring speed was typically fixed at 500 rpm. After a fixed time, the reaction was quickly terminated by cooling the reactor to room temperature. The liquid products were analyzed by high-performance liquid chromatography (Shimazu LC-20A)

equipped with an refractive index (RI) detector and a Shodex SUGARSH-1011 column (8 mm × 300 mm) using a dilute H_2SO_4 aqueous solution as a mobile phase. The conversion of HMF and the selectivity of each product were defined as the molar percentage of HMF converted and the molar percentage of each product in HMF converted, respectively. Both the conversion and selectivity were calculated on a carbon basis.

3. RESULTS AND DISCUSSION

3.1. Structure and Unique Catalytic Behavior of Au-Pd/CNT for the Base-Free Aerobic Oxidation of HMF into FDCA. The actual loading amounts of (Au + Pd) and molar ratios of Au/Pd in the Au-Pd catalysts loaded on different supports, which have been measured by the ICP-MS, are displayed in Table 1. The results show that almost all of the Au-Pd nanoparticles in the colloids can be immobilized onto the support by the colloidal immobilization method and the Au/Pd molar ratios in these catalysts are also close to 1/1, which has been used in the preparation stage. The specific surface areas of these catalysts measured by the N_2 physisorption were similar to those of the corresponding supports (Supporting Information Table S2).

The TEM measurements for these catalysts clarified that the mean sizes of Au-Pd (Au/Pd = 1/1) nanoparticles loaded on different supports were similar, being 2.4-2.7 nm except for the Au-Pd/SiO_2, which possessed a slightly larger mean size of Au-Pd particles (Table 1, see Supporting Information Figure S1 for TEM images of the catalysts). Figure 1 shows a representative TEM image for the Au-Pd/CNT catalyst. We have performed the line-scan energy-dispersive X-ray spectroscopy (EDS) analyses for several Au-Pd nanoparticles located on CNT. The EDS analyses reveal that Au and Pd elements are uniformly distributed in all these nanoparticles (see

Figures 1b and 1c for two Au-Pd particles with sizes of ~4.0 and ~2.3 nm, respectively). This suggests that the nanoparticles over this catalyst are composed of Au-Pd alloy.

Our XPS studies showed that the binding energy of Au $4f_{7/2}$ in the Au-Pd/CNT catalyst was 84.0 eV, which was ~0.4 eV lower than that in the Au/CNT (84.4 eV), whereas the binding energy of Pd $3d_{5/2}$ in the bimetallic catalyst was 336 eV, higher than that in the Pd/CNT catalyst (335.6 eV) (Figure 2). These shifts of binding energies of Au $4f_{7/2}$ and Pd $3d_{5/2}$ further confirm the formation of alloy nanoparticles between Au and Pd, and may suggest the electron transfer from Pd to Au.[65]

Catalytic studies demonstrated that the support played crucial roles in the aerobic oxidation of HMF over the supported Au-Pd catalysts (Table 1). The combination of the catalytic performances with the specific surface areas (Supporting Information Table S2) clearly suggests that the surface area is not a key factor determining the catalytic behaviors. The employment of metal oxides except for MgO as the supports led to the formations of 2,5-diformylfuran (DFF) and 5-formyl-2-furancarboxylic acid (FFCA) but almost no FDCA irrespective of the specific surface areas. When MgO, a strong solid base, was used as the support, HMF was completely converted with a FDCA selectivity of 99%. However, the Au-Pd/MgO catalyst was unstable during the reaction and could not be used recyclably due to the dissolution of MgO into the reaction solution containing FDCA (Figure 3a). We confirmed that the Au-Pd/HT catalyst, which also showed better FDCA yield, underwent similar deactivation during the repeated uses (Figure 3b).

The Au-Pd nanoparticles loaded on the carbon materials showed higher HMF conversions and FDCA selectivities than those loaded on metal oxides except for MgO or HT (Table 1). In particular, the CNT was an excellent support for the aerobic oxidation of HMF to FDCA in water;

the HMF conversion and FDCA selectivity over the Au-Pd/CNT catalyst reached 100% and 94%, respectively. It should be noted that Prati and co-workers recently reported that Au-Pd nanoparticles loaded on an activated carbon support could also catalyze the aerobic oxidation of HMF to FDCA with a high efficiency; an FDCA yield of >99% could be obtained for the conversion of HMF with a concentration of 0.15 M under relatively mild conditions (333 K, 4 h).[59] However, the presence of a base additive, i.e., NaOH, is indispensable for the conversion of HMF under such mild conditions.[59] We have demonstrated that CNT is a unique support for the aerobic oxidation of HMF to FDCA in the absence of a base additive. Nevertheless, it should be mentioned that relatively higher temperatures and longer reaction times are required to obtain a full conversion of HMF under base-free conditions. We have also performed the aerobic oxidation of HMF with a higher concentration (0.15 M), and an FDCA yield of 91% has been obtained over the Au-Pd/CNT catalyst after 18 h of reaction at 373 K (Table 1). Moreover, as compared to the Au-Pd/MgO and Au-Pd/HT, the Au-Pd/CNT was much more stable during the recycling uses (Figure 4). Although the selectivity of FDCA decreased slightly in the initial three recycles, both the HMF conversion and FDCA selectivity were sustained in the further recycling uses. Thus, the Au-Pd/CNT is a highly efficient and recyclable catalyst for the conversion of HMF to FDCA under base-free conditions.

Almost no conversion of HMF was observed over CNT alone. DFF and FFCA were the major products over the catalyst with a lower loading of Au-Pd nanoparticles (Table 2). The HMF conversion and FDCA selectivity increased with the loading of Au-Pd nanoparticles on CNTs, both reaching >90% as the Au-Pd loading became ≥0.67 wt%. These observations confirm that the Au-Pd alloy nanoparticle is essential for the aerobic oxidation of HMF to FDCA. The Au-Pd/CNT catalyst could also catalyze the oxidation of HMF with air; HMF conversion and FDCA

selectivity reached 100% and 96%, respectively, after a reaction under an air pressure of 1.0 MPa and 373 K for 12 h. These results further demonstrate that the Au-Pd/CNT is a promising catalyst for the base-free aerobic oxidation of HMF to FDCA in water.

3.2. Support-Enhanced Adsorption Effect for the Au-Pd/CNT-Catalyzed Aerobic Oxidation of HMF into FDCA. The results in Table 1 clearly show that the support plays a key role in the aerobic oxidation of HMF to FDCA. Generally, a catalyst support may offer better dispersions of active sites and modify the electronic or geometric state of the active metal nanoclusters, consequently influencing the catalytic behavior.[66,67] Another important effect of the support, which is usually overlooked, is the enhancement of the adsorption of the reactant and the reaction intermediates. This effect becomes particularly vital for the heterogeneous catalytic conversion of organic molecules in water medium. The preferential adsorption of water and polar products such as acids on the hydrophilic sites of supports may hamper the access of the organic reactants or reaction intermediates to the active sites and thus limit the catalytic performance and the catalyst stability. The enhancement of the hydrophobicity of catalyst surfaces is a useful strategy to increase the catalyst performance for such kind of reactions.[68-71] Thus far, the organic modification of inorganic supports is typically employed for the preparation of hydrophobic catalysts,[68-71] but the recyclability of these catalysts is still problematic. Moreover, few studies have been devoted to finely tuning the organic functional groups on catalyst surfaces.

The relatively better catalytic performances of carbon material-supported Au-Pd catalysts (Table 1) allow us to speculate that the organic feature of the support may contribute to the adsorption of the organic reactant (HMF) and possible intermediates (DFF and FFCA) from water solution. In particular, we speculate that the sp^2-bonded carbon networks on CNT or GO surfaces may favor the interaction with the aromatic furan ring in the reactant or intermediates,

and thus facilitate the reaction. To confirm this point, we have measured the adsorption amounts of HMF and the possible reaction intermediates, i.e., DFF and FDCA, on different supports. The combination of the adsorption results for different supports (Supporting Information Table S3) with the surface areas of these supports (Supporting Information Table S1) suggests that the surface area may influence the adsorption but is not the determining factor. The carbon materials, in particular CNT, showed higher adsorption amounts of these compounds (especially DFF and FFCA) than the metal oxides except for MgO (Supporting Information Table S3). MgO exhibited an adsorption amount of FFCA comparable to CNT. It is easy to understand that MgO can adsorb a larger amount of FFCA because of the acid-base interaction. The combination of the results in Table 1 and Supporting Information Table S3 allows us to propose that the difference in the adsorption ability of support may largely affect the catalytic behavior of the supported Au-Pd catalysts.

We have also performed co-adsorption studies for three combinations, i.e., (HMF + DFF), (HMF + FFCA), and (HMF + FDCA), over CNTs. Both HMF and the possible reaction intermediate (DFF or FFCA) could be adsorbed simultaneously on CNTs, and the adsorption amount of either DFF or FFCA was higher than that of HMF under the conditions used for the co-adsorption (Supporting Information Table S4), suggesting that CNTs exhibited better adsorption capacity for these possible reaction intermediates. On the other hand, the adsorption amount of FDCA was significantly lower than that of HMF. In other words, the product, FDCA, did not adsorb strongly on CNT surfaces. This would favor both the conversion of HMF and the selectivity of FDCA. We further clarified that the co-adsorption of the possible intermediate (particularly FFCA) or product (FDCA) decreased the adsorption amount of HMF, but such a decrease was not very serious (Supporting Information Table S4).

Many studies have pointed out that the oxygen-containing functional groups (including phenol, carbonyl/quinone, anhydride, ester, lactone, and carboxyl groups) on the surfaces of carbon materials, particularly CNTs, play significant roles in the catalysis of carbon-based materials.[72-84] Rass et al. once reported that the oxygenated functional groups such as carboxyl groups on activated carbon support were detrimental to the Pt-catalyzed aerobic oxidation of HMF to FDCA in the presence of a base additive.[82] The pretreatment of CNTs with different methods can create different types of functional groups. It is expected that the tuning of functional groups on CNT surfaces may regulate the adsorption amount of HMF or the possible intermediates and thus affect the catalytic behavior.

We have functionalized CNT surfaces by HNO_3 and H_2O_2 in addition to the standard pretreatment by 5 wt% HCl aqueous solution. Since different surface oxygen-containing groups can be decomposed to CO and/or CO_2 at different temperatures, the temperature-programmed desorption (TPD) is a powerful technique to quantify the concentration of functional groups on carbon materials.[85] From the CO and CO_2 desorption peaks in TPD profiles for the Au-Pd/CNT catalysts with CNTs pretreated by different methods (Supporting Information Figure S2), we have estimated the relative concentrations of various functional groups, and the results are summarized in Table 3. It should be noted that the relative concentration of the strongest peak for each functional group among the four differently pretreated CNT samples has been normalized to 100%. For the catalyst with CNT pretreated by 5 wt% HCl (standard pretreatment), the relative concentrations of phenol and carbonyl/quinone groups were higher, while those of carboxyl, anhydride, ester, and lactone groups were lower.

The oxidative treatment of CNTs by concentrated HNO_3 increased the concentrations of carboxyl, anhydride, ester, and lactone groups, and decreased those of phenol and

carbonyl/quinone groups. On the other hand, the treatment by H_2O_2 increased not only the concentrations of anhydride, ester, and lactone groups but also those of phenol and carbonyl/quinone groups. However, the concentration of carboxyl group was not significantly altered. Our XPS studies also suggest that the CNT pretreated by concentrated HNO_3 possesses higher fraction of carboxyl groups, whereas the fraction of carbonyl/quinone groups becomes higher over the CNT pretreated by H_2O_2 (Supporting Information Figure S3 and Table S5).

As compared to the Au-Pd/CNT (Au/Pd = 1/1) catalyst with CNT pretreated by 5 wt% HCl, the catalysts with CNTs further treated by HNO_3 showed lower HMF conversions and FDCA selectivities (Figure 5). The conversion of HMF decreased to 20% and no FDCA was formed when 68 wt% HNO_3 was used for the treatment of CNTs. On the other hand, the treatment of CNTs by H_2O_2 afforded a more efficient catalyst, and the FDCA yield reached 95% even after 10 h of reaction at 373 K under base-free conditions.

As confirmed by TEM measurements, there were no significant differences in the mean sizes of Au-Pd alloy nanoparticles over the catalysts with CNTs pretreated differently (Supporting Information Figure S4). N_2 physisorption measurements showed that the surface areas and pore volumes for the catalysts with CNTs pretreated by different methods were in the ranges of 105~116 $m^2\ g^{-1}$ and 0.36-0.39 $cm^2\ g^{-1}$, respectively (Supporting Information Table S6). This indicated that the pretreatment by concentrated HNO_3 or H_2O_2 did not lead to significant changes in the porous structure of CNT. We further performed Raman spectroscopic measurements. The ratios of the integrated intensities of the D-band at 1340-1380 cm^{-1} and the G-band at 1570-1600 cm^{-1}, which could be used to characterize the defects in the graphitic structure of carbon materials,[86] were in the range of 1.12-1.19 for the catalysts with CNTs pretreated by different methods (Supporting Information Figure S5 and Table S6). This further confirms that the CNT

structure does not undergo significant changes after the pretreatment used in this work. Thus, we can conclude that the type of functional groups on CNTs plays pivotal roles in determining the catalytic performance of the supported Au-Pd catalyst. The correlation of the catalytic performance (Figure 5) with the relative concentrations of different types of functional groups on CNTs (Table 3 and Supporting Information Table S5) suggests that the carboxyl group is unfavorable for HMF conversion and FDCA formation, whereas the carbonyl/quinone and/or phenol group enhances FDCA formation.

To gain more insights into the effects of the functional groups on carbon materials on the catalytic behaviors, we have further investigated the catalysts with CNFs pretreated by different methods. In addition to that pretreated by 5 wt% HCl (standard pretreatment), the CNFs pretreated by 68 wt% HNO_3 and 30 wt% H_2O_2 were also used as the catalyst supports for the Au-Pd nanoparticles (loading amount = 1.0 wt%, Au/Pd = 1/1). The catalytic studies for these samples in the aerobic oxidation of HMF at 373 K showed that the catalyst with the CNF pretreated by 68 wt% HNO_3, on which a higher density of carboxyl groups could be generated, exhibited much lower conversion of HMF and lower selectivity to FDCA than the catalyst with the CNF pretreated by 5 wt% HCl (Supporting Information Table S7). On the other hand, over the Au-Pd/CNF catalyst with the CNF pretreated by H_2O_2, on which a higher density of carbonyl/quinone and phenol groups could be generated, significantly higher HMF conversion and FDCA selectivity were obtained (Supporting Information Table S7). Thus, the carboxyl groups on CNFs play a negative role in the catalytic reaction, while the carbonyl/quinone and/or phenol groups favor the conversion of HMF to FDCA. These results are in good agreement with those obtained for the Au-Pd/CNT catalysts with CNTs pretreated by different methods and

further confirm the important roles of the functional groups on the surfaces of carbon materials in the aerobic oxidation of HMF under base-free conditions.

We have measured the adsorption amounts of HMF and the two possible intermediates (DFF and FFCA) on the CNTs pretreated by different methods. As compared to the CNT pretreated by 5 wt% HCl, the CNTs further treated by 30 wt% and 68 wt% HNO_3 exhibited lower adsorption amounts of both HMF and the possible intermediates (Table 4). On the other hand, the adsorption of HMF and the possible intermediates was enhanced on the CNT pretreated by H_2O_2. Thus, it becomes clear that the carbonyl/quinone and/or phenol groups enhance the adsorption of HMF and the possible intermediates onto the CNT surfaces, whereas the carboxyl groups are disadvantageous to the adsorption of these molecules. These results further suggest that the adsorption ability of the support for HMF and the possible reaction intermediates contributes significantly to the catalysis for the aerobic oxidation of HMF to FDCA in water.

To gain further evidence for the role of the surface functional groups, we have studied the influence of the modification of the Au-Pd/Al_2O_3 (Au/Pd = 1/1) catalyst by benzoic acid, phenol, and quinone, which may function as model organic molecules of different functional groups. The Au-Pd/Al_2O_3 catalyst without modification showed a HMF conversion of 34%, and the major products were DFF and FFCA. The modification by benzoic acid decreased the HMF conversion and FDCA yield (Table 5). On the other hand, the modification of the Au-Pd/Al_2O_3 with quinone significantly accelerated both HMF conversion and FDCA selectivity. The FDCA yield was also improved to some extent by the modification with phenol. These observations agree well with the results obtained for the Au-Pd/CNT catalysts containing different functional groups on CNT surfaces. Furthermore, the result in Table 5 may suggest that the quinone groups play more positive effects on FDCA formation than the phenol groups on CNT-supported catalysts.

Therefore, we have clearly demonstrated the importance of the adsorption of the reactant and possible reaction intermediates by using the functionalized CNT supports. We expect that the effective control of the support-enhanced adsorption effect may finely tune the reaction rates in different elementary steps and may be further utilized for the design of efficient heterogeneous catalysts for the aerobic oxidation of organic molecules in water.

3.3. Alloying Effect for the Au-Pd/CNT-Catalyzed Aerobic Oxidation of HMF into FDCA. To gain insights into the alloying effect, we have investigated the CNT-supported bimetallic catalysts with different Au/Pd ratios as well as monometallic catalysts. The ICP-MS measurements for these catalysts confirm that the loading amounts of Au and/or Pd and the molar ratios of Au/Pd in the catalysts are close to those used for preparation (Table 6). Our TEM measurements reveal that the bimetallic or monometallic nanoparticles are homogeneously dispersed on CNTs over these catalysts (Supporting Information Figure S6). The mean sizes of nanoparticles over these catalysts are almost the same (2.5-2.7 nm). Table 6 shows that the CNT-supported monometallic Au or Pd catalyst is less active and selective for the oxidation of HMF to FDCA than the supported alloy catalysts. It is noteworthy that 5-hydroxymethyl-2-furancarboxylic acid (HMFCA), the product from the oxidation of the aldehyde group in HMF, was formed over the Au/CNT catalysts, whereas this product was not observed over the other catalysts in Table 6. Byproducts from ring-opening and degradation were also formed with higher selectivities over the Au/CNT catalyst under our reaction conditions. Significant synergistic effects exist between Au and Pd in the alloys on enhancing the HMF conversion and FDCA selectivity. The catalyst with an Au/Pd molar ratio of 1/1 exhibits the best performance for the conversion of HMF to FDCA.

The time-course analysis for the conversion of HMF can provide information on the reaction paths and reaction mechanism. The result for the Au-Pd/CNT (Au/Pd = 1/1) catalyst in Figure 6 shows that the selectivity to DFF decreases quickly with reaction time in the initial 4 h and that to FFCA begins to decrease as the reaction time exceeds 4 h, while the selectivity to FDCA increases monotonically with reaction time. These observations clearly indicate a tandem pathway for the conversion of HMF to FDCA via DFF and FFCA (Scheme 1a).

We also investigated the time courses for the conversion of HMF over the CNT-supported monometallic catalysts to gain deeper insights into the alloying effect on the reaction mechanism. The result for the Pd/CNT catalyst (Supporting Information Figure S7) suggests the same tandem reaction pathway with that for the Au-Pd/CNT catalyst (Scheme 1a). However, the Au/CNT behaved differently during the oxidation of HMF. HMFCA was formed with considerable selectivities at the initial reaction stage over the Au/CNT catalyst (Figure 7), indicating that HMFCA was a major primary product together with DFF (Scheme 1b). The ring-opening and degradation products (including gluconic acid, glucuronic acid, succinic acid, glycolic acid, and formic acid) were also formed over the Au/CNT catalyst, and the selectivity of these byproducts increased at the expense of the HMFCA selectivity at longer reaction times (Figure 7).

We have further performed the conversion of HMFCA over the Au/CNT catalyst and clarified that the ring-opening and degradation products stem from HMFCA (Supporting Information Figure S8). The ring-opening of HMFCA occurs first and then the degradation takes place over the Au/CNT catalyst under base-free conditions, leading to the very low FDCA selectivity (Table 6 and Figure 7). On the other hand, HMFCA was not formed over the Pd/CNT and the Au-Pd/CNT catalysts.

We further performed the aerobic oxidations of DFF and FFCA, two major intermediates for FDCA formation, over the Au/CNT, Pd/CNT, and Au-Pd/CNT (Au/Pd = 1/1) catalysts. The conversion of DFF produced FFCA and FDCA, while FDCA was the only product from FFCA over these catalysts (Supporting Information Figures S9 and S10), further confirming the reaction pathways in Scheme 1.

The rates of HMF, DFF, and FFCA conversions over the Au/CNT, Pd/CNT, and Au-Pd/CNT (Au/Pd = 1/1) catalysts have been evaluated using the results obtained for the oxidation of these substrates at the initial reaction stage. As summarized in Table 7, the addition of Pd to Au/CNT to form Au-Pd alloy significantly accelerates the oxidation of the hydroxyl group of HMF, forming DFF (Scheme 1, Step 1), and retards the path for HMFCA formation (Scheme 1, Step 1'). The incorporation of Pd to the supported Au catalyst also enhanced the conversions of DFF and FFCA. In particular, the oxidation of FFCA (Scheme 1, Step 3) was significantly accelerated and the rate of FFCA conversion increased ~220 times owing to the presence of Pd. It is noteworthy that the Au/CNT catalyst is almost inactive for the conversion of FFCA under our base-free conditions. This is quite different from the result obtained for the supported Au catalysts in the presence of a base, where the conversion of FFCA is a fast step.[42-47] The base, i.e., OH^-, has been reported to accelerate the conversion of FFCA to FDCA via a hemiacetal intermediate.[42-47]

Thus, we have clearly demonstrated that the use of the supported Au-Pd alloy instead of monometallic Au catalyst is a useful strategy to avoid the formation of HMFCA, which leads to the ring-opening and degradation reactions under base-free conditions, and to direct the formation of FDCA via DFF and FFCA. Furthermore, the incorporation of Pd enhances the

conversion of FFCA to FDCA, which is a quite difficult elementary step under base-free conditions.

On the other hand, the reaction pathways were the same for the Pd/CNT and Au-Pd/CNT catalysts (Scheme 1a). However, as compared to the Pd/CNT, the supported alloy catalyst exhibited higher activities for all the three tandem reaction steps (Table 7). In particular, the rate for the oxidation of HMF to DFF over the supported alloy catalyst was ~8 times higher than that over the supported Pd catalyst. This means that the embedding of Au into Pd can also significantly accelerate the oxidation of the hydroxyl group in HMF.

4. CONCLUSIONS

We have reported for the first time that CNT-supported Au-Pd alloy nanoparticles are highly efficient and recyclable heterogeneous catalysts for the aerobic oxidation of HMF to FDCA in water under base-free conditions. It has been demonstrated that the support-enhanced adsorption effect and the alloying effect mainly contribute to the realization of the base-free oxidation of HMF to FDCA. Enhanced adsorption of HMF and the intermediates (i.e., DFF and FFCA) from water onto the functionalized CNT surfaces contributes significantly to the aerobic oxidation of HMF to FDCA. We have clarified that the carbonyl/quinone and phenol (especially the former) groups on CNT surfaces facilitate the adsorption of HMF and the intermediates, and thus accelerate the formation of FDCA. On the other hand, the carboxyl groups on CNTs are unfavorable for the adsorption of HMF and reaction intermediates, and thus, retard the reaction. In addition to the support-enhanced adsorption effect, significant synergistic effects also exist between Au and Pd in the alloy for the oxidation of HMF to FDCA in three tandem steps via DFF and FFCA. The CNT-supported Au monometallic catalyst preferentially catalyzes the

oxidation of the aldehyde group in HMF, forming HMFCA, which mainly undergoes ring-opening and degradation reactions to byproducts under base-free conditions. The use of the supported Au-Pd alloy nanoparticles changes the main route from HMFCA formation to DFF formation by accelerating the oxidation of the hydroxyl group in HMF. DFF is then oxidized into FDCA via FFCA. The incorporation of Pd further enhances the oxidation of FFCA to FDCA, a difficult elementary step over the supported monometallic Au catalyst under base-free conditions. On the other hand, although the Pd/CNT can also catalyze the oxidation of HMF to FDCA via DFF and FFCA, the Au-Pd/CNT catalyst exhibits higher rates in the three tandem elementary steps. In particular, the rate of the oxidation of the hydroxyl group in HMF is significantly accelerated by the presence of Au. We believe that these insights into the support-enhanced adsorption effect and the alloying effect can be applied to other oxidative transformations, in particular those involving tandem oxidation of organic compounds with different functional groups in water.

ASSOCIATED CONTENT

Supporting Information

Specific surface areas and structural information of supports, Specific surface areas and pore volumes of supported catalysts, TEM micrographs for Au-Pd nanoparticles loaded on different supports, Adsorption amounts of HMF, DFF, and FDCA on supports, Co-adsorption of HMF and possible reaction intermediates or products, TPD profiles, XPS spectra, TEM micrographs, N_2 physisorption results, and Raman spectra for Au-Pd/CNT catalysts with CNTs pretreated by different methods, Catalytic performances of Au-Pd/CNF catalysts with CNFs pretreated by different methods, TEM micrographs for CNT-supported bimetallic catalysts with different Au/Pd ratios, Time course for the conversion of HMF over Pd/CNT, Time course for the conversion of HMFCA over Au/CNT, Time courses for the conversions of DFF and FFCA over Au/CNT, Pd/CNT, and Au-Pd/CNT.

AUTHOR INFORMATION

Corresponding Author

*E-mail: wangye@xmu.edu.cn; zhangqh@xmu.edu.cn.

Notes

The authors declare no competing financial interest.

ACKNOWLEDGMENT

This work was supported by the Natural Science Foundation of China (Nos. 21173172, 21103143, 21033006, and 21161130522), the National Basic Research Program of China (No. 2013CB933100), the Research Fund for the Doctoral Program of Higher Education

(2013012113001), and the Program for Innovative Research Team in Chinese Universities (No. IRT1036).

REFERENCES

1 Corma, A.; Iborra, S.; Velty, A. *Chem. Rev*. **2007**, *107*, 2411–2502.

2 Dhepe, P.; Fukuoka, A. *ChemSusChem* **2008**, *1*, 969–975.

3 Van de Vyver, S.; Geboers, J.; Jacobs, P.; Sels, B. *ChemCatChem* **2011**, *3*, 82–94.

4 Kobayashi, H.; Ohta, H.; Fukuoka, A. *Catal. Sci. Technol*. **2012**, *2*, 869–883.

5 Deng, W.; Zhang, Q.; Wang, Y. *Dalton Trans*. **2012**, *41*, 9817–9831.

6 Ruppert, A.; Weinberg, K.; Palkovits, R. *Angew. Chem. Int. Ed*. **2012**, *51*, 2564–2601.

7 Wang, A.; Zhang, T. *Acc. Chem. Res*. **2013**, *46*, 1377–1386.

8 Román-Leshkov, Y.; Chheda, J.; Dumesic, J. *Science* **2006**, *312*, 1933–1937.

9 Zhao, H.; Holladay, J.; Brown, H.; Zhang, Z. *Science* **2007**, *316*, 1597–1600.

10 Chheda, J.; Huber, G.; Dumesic, J. *Angew. Chem. Int. Ed*. **2007**, *46*, 7164–7183.

11 Binder, J.; Raines, R. *J. Am. Chem. Soc*. **2009**, *131*, 1979–1985.

12 Zakrzewska, M.; Bogel-Łukasik, E.; Bogel-Łukasik, R. *Chem. Rev.* **2011**, *111*, 397–417.

13 Rosatella, A.; Simeonov, S.; Frade, R.; Afonso, C. *Green Chem.* **2011**, *13*, 754–793.

14 Werpy, T.; Petersen, G.; Aden, A.; Bozell, J.; Holladay, J.; White, J.; Jones, S.; Top Value Added Chemicals From Biomass, **2004**, Vol. 1, 26-28. Available at: http://www1.eere.energy.gov/bioenergy/pdfs/35523.pdf.

15 Eerhart, A.; Faaij, A.; Patel, M. *Energy Environ. Sci*. **2012**, *5*, 6407–6422.

16 Hasgimi, A.; Hutchings, G. J. *Angew. Chem. Int. Ed*. **2006**, *45*, 7896–7936.

17 Corma, A.; Garcia, H. *Chem. Soc. Rev*. **2008**, *37*, 2096–2126.

18 Takei, T.; Akita, T.; Nakamura, I.; Fujitani, T.; Okumura, M.; Okazaki, K.; Huang, J.; Ishida, T.; Haruta, M. *Adv. Catal*. **2012**, *55*, 1–126.

19 Haruta, M. *Angew. Chem. Int. Ed*. **2014**, *53*, 52–56.

20 Haruta, M.; Yamada, N.; Kobayashi, T.; Iijima, S. *J. Catal.* **1989**, *115*, 301–309.

21 Hayashi, T.; Tanaka, K.; Haruta, M. *J. Catal.* **1998**, *43*, 33–39.

22 Lee, W.; Zhang, R.; Akatay, M.; Baertsch, C. D.; Stach, E. A.; Ribeiro, F. H.; Delgass, W. N. *ACS Catal.* **2011**, *1*, 1327–1330.

23 Xu, X. J.; Fu, Q.; Guo, X. G.; Bao, X. H. *ACS Catal.* **2013**, *3*, 1810–1818.

24 Sun, B.; Feng, X. Z.; Yao, Y.; Su, Q.; Ji, W. J.; Au C. T. *ACS Catal.* **2013**, *3*, 3099–3105.

25 Prati, L.; Rossi, M. *J. Catal.* **1998**, *176*, 552–560.

26 Pina, C.; Falletta, E.; Prati, L.; Rossi, M. *Chem. Soc. Rev.* **2008**, *37*, 2077–2095.

27 Sun, K. Q.; Hong, Y. C.; Zhang, G. R.; Xu, B. Q. *ACS Catal.* **2011**, *1*, 1336–1346.

28 Liu, Y. M.; Tsunoyama , H; Akita, T.; Xie, S. H.; Tsukuda T. *ACS Catal.* **2011**, *1*, 2–6.

29 Davis, S.; Ide, M.; Davis, R. *Green Chem.* **2013**, *15*, 17–45.

30 Dimitratos, N.; Villa, A.; Wang, D.; Porta, F.; Su, D.; Prati, L. *J. Catal.* **2006**, *244*, 113–121.

31 Enache, D.; Edwards, J.; Landon, P.; Solsona-Espriu, B.; Carley, A.; Herzing, A.; Wa-tanabe, M.; Kiely, C.; Knight, D.; Hutchings, G. J. *Science* **2006**, *311*, 362–365.

32 Zhang, H.; Watanabe, T.; Okumura, M.; Haruta M.; Toshima, N. *Nat. Mater.* **2012**, *11*, 49–52.

33 Tongsakul, D.; Nishimura, S.; Ebitani, K. *ACS Catal.* **2013**, *3*, 2199–2207.

34 Sankar, M.; Dimitratos, N.; Miedziak, P.; Wells, P.; Kiely, C.; Hutchings, G. J. *Chem. Soc. Rev*. **2012**, *41*, 8099–8139.

35 Freakley, S. J.; Piccinini, M.; Edwards, J. K.; Ntainjua, E. N.; Moulijn, J. A.; Hutchings, G. J. *ACS Catal.* **2013**, *3*, 487–501.

36 Kesavan, L.; Tiruvalam, R.; Ab Rahim, M. H.; bin Saiman, M. I.; Enache, D. I.; Jenkins, R. L.; Dimitratos, N.; Lopez-Sanchez, J. A.; Taylor, S. H.; Knight, D. W.; Kiely, C. J.; Hutchings, G. J. *Science* **2011**, *331*, 195–199;

37 Brett, G.; He, Q.; Hammond, C.; Miedziak, P. J.; Dimitratos, N.; Sankar, M.; Herzing, A. A.; Conte, M.; Lopez-Sanchez, J. A.; Kiely, C. J.; Knight, D. W.; Taylor, S. H.; Hutchings, G. J. *Angew. Chem., Int. Ed.* **2011**, *50*, 10136–10139.

38 Edwards, J. K.; Pritchard, J.; Piccinini, M .; Shaw, G.; He, Q.; Carley, A. F.; Kiely, C. J.; Hutchings, G. J. *J. Catal.* **2012**, *292*, 227–238.

39 Hutchings G. J.; Kiely, C. J. *Acc. Chem. Res.* **2013**, *46*, 1759–1772.

40 Pritchard J.; Piccinini M.; Tiruvalam R.; He Q.; Dimitratos N.; Lopez-Sanchez J. A.; Morgan D. J.; Carley A. F.; Edwards J. K.; Kiely, C. J.; Hutchings G. J. *Catal. Sci. Technol.* **2013**, *3*, 308–317.

41 Edwards, J. K.; Freakley, S. J.; Carley, A. F.; Kiely, C. J.; Hutchings, G. J. *Acc. Chem. Res.* **2014**, *47*, 845–854.

42 Gorbaney, Y.; Klitgaard, S.; Woodley, J.; Chris-tensen, C.; Riisager, A. *ChemSusChem* **2009**, *2*, 672–675.

43 Casanova, O.; Corma, A. *ChemSusChem* **2009**, *2*, 1138–1144.

44 Guppta, N.; Nishimura, S.; Takagaki, A.; Ebitani, K. *Green Chem*. **2011**, *13*, 824–827.

45 Davis, S.; Zope, B.; Davis, R. *Green Chem.* **2012**, *14*, 143–147.

46 Zope, B.; Davis, S.; Davis, R. *Top. Catal.* **2012**, *55*, 24–32.

47 Cai, J. ; Ma, H.; Zhang, J.; Song, Q.; Du, Z. ; Huang, Y.; Xu, J. *Chem. Eur. J.* **2013**, *19*, 14215–14223.

48 Vinke, P.; Van Gam, H.; Van Bekkum, H. *Stud. Surf. Sci. Catal*. **1990**, *55*, 147–158.

49 Lilga, M.; Hallen, R.; Gray, M. *Top. Catal*. **2010**, *53*, 1264–1269.

50 Gorbanev, Y.; Kegnæs, S.; Riisager, A. *Catal. Lett.* **2011**, *141*, 1752–1760.

51 Davis, S.; Houk, L.; Tamargo, E.; Datye, A.; Davis, R. *Catal. Today* **2011**, *160*, 55–60.

52 Vuyyuru, K.; Strasser, P. *Catal. Today* **2012**, *195*, 144–154.

53 Nie, J.; Xie, J.; Liu, H. *J. Catal*. **2013**, *301*, 83–91.

54 Taarning, E. ; Nielsen, I.; Egeblad, K.; Madsen, R.; Christensen, C. *ChemSusChem* **2008**, *1*, 75–78.

55 Casanova, O.; Iborra, S.; Corma, A. *J. Catal*. **2009**, *265*, 109–116.

56 Pinna, F.; Olivo, A.; Trevisan, V.; Menegazzo, F.; Signoretto, M.; Manzoli, M.; Boccuzzi, F. *Catal. Today* **2013**, *203*, 196–201.

57 Guo, Z.; Liu, B.; Zhang, Q.; Deng, W.; Wang, Y.; Yang, Y. *Chem. Soc. Rev.* **2014**, *43*, 3480–3524.

58 Pasini, T.; Piccinini, M.; Blosi, M.; Albonetti, S.; Dimi-tratos, N.; Lopez-Sanchez, J. ; Sankar, M.; He, Q.; Kiely, C.; Hutchings, G.; Cavani, F. *Green Chem.* **2011**, *13*, 2091–2099.

59 Villa, A.; Schiavoni, M.; Campisi, S.; Veith, C.; Prati, L. *ChemSusChem* **2013**, *6*, 609–612.

60 Chen, P.; Zhang, H.; Lin, G.; Hong, Q.; Tsai, K. *Carbon* **1997**, *35*, 1495–1501.

61 Fang, W.; Chen, J.; Zhang, Q.; Deng, W.; Wang, Y. *Chem. Eur. J*. **2011**, *17*, 1247–1256.

62 Fan, W.; Lai, Q.; Zhang, Q.; Wang, Y. *J. Phys. Chem. C* **2011**, *115*, 10694–10701.

63 Peng, Y.; Liu, H. *Ind. Eng. Chem. Res.* **2006**, *45*, 6483–6488.

64 Lopez-Sanchez, J.; Dimitratos, N.; Hammond, C.; Brett, G.; Kesavan, L.; White, S.; Miedziak, P.; Tiruvalam, R.; Jenkins, R.; Carley, A.; Knight, D.; Kiely, C.; Hutchings, G. J. *Nat. Chem*. **2011**, *3*, 551–556.

65 Griffin, M.; Rodriguez, A.; Montemore, M.; Monnier, J.; Williams, C.; Medlin, J. *J. Catal*. **2013**, *307*, 111–120.

66 Ta, N.; Liu, J.; Chenna, S.; Crozier, P.; Li, Y.; Chen, A.; Shen, W. *J. Am. Chem. Soc*. **2012**, *134*, 20585–20588.

67 Wang, F.; Ueda, W.; Xu, J. *Angew. Chem. Int. Ed*. **2012**, *16*, 3883–3887.

68 Klein, S.; Maier, W. *Angew. Chem. Int. Ed. Engl*. **1996**, *35*, 2230–2233.

69 Lin, K.; Pescarmona, P.; Houthoofd, K.; Liang, D.; Van Tendeloo, G.; Jacobs, P. *J. Catal.* **2009**, *263*, 75–82.

70 Chen, C.; Xu, J.; Zhang, Q.; Ma, Y.; Zhou, L.; Wang, M. *Chem. Commum.* **2011**, *47*, 1336–1338.

71 Wang, M.; Wang, F.; Ma, J.; Che, C.; Shi, S.; Xu, J. *Chem. Commun*. **2013**, *49*, 6623–6625.

72 Zhang, J.; Liu, X.; Blume, R.; Zhang, Z.; Schlögl, R.; Su, D. *Science* **2008**, *322*, 73–77.

73 Kang, J.; Zhang, S.; Zhang, Q.; Wang, Y. *Angew. Chem. Int. Ed.* **2009**, *48*, 2565–2568.

74 Su, D.; Zhang, J.; Frank, B.; Thomas, A.; Wang, X.; Paraknowitsch, J.; Schlögl, R. *ChemSusChem* **2010**, *3*, 169–180.

75 Figueiredo, J.; Pereira, M. *Catal. Today* **2010**, *150*, 2–7;

76 Deng, W.; Liu, M.; Tan, X.; Zhang, Q.; Wang, Y. *J. Catal.* **2010**, *271*, 22–32.

77 Su, D.; Perthoner, S.; Centi, G. *Chem. Rev*. **2013**, *113*, 5782–5816.

78 Rodrigues, E. G.; Pereira, M. F. R.; Chen, X.; Delgado, J. J.; Orfao, J. J. M. *J. Catal.* **2011**, *281*, 119–127.

79 Wepasnick, K. A.; Smith, B. A.; Schrote, K. E.; Wilson, H. K.; Diegelmann, S. R.; Fairbrother, D. H. *Carbon* **2011**, *49*, 24–36.

80 Gosselink, R. W.; van den Berg, R.; Xia, W.; Muhler, M.; de Jong, K. P.; Bitter, J. H. *Carbon* **2012**, *50*, 4424–4431.

81 Sanchez-Sanchez, A.; Suarez-Garcia, F.; Martinez-Alonso, A.; Tascon, J. M. D. *Carbon* **2013**, *62*, 193–203.

82 Rass, H. A.; Essayem, N.; Besson, M. *Green Chem.* **2013**, *15*, 2240–2251.

83 Qi, W.; Liu, W.; Zhang B.; Gu, X.; Guo, X.; Su, D. *Angew. Chem. Int. Ed.* **2013**, *52*, 14224–14228.

84 Wang, D.; Su, D. *Energy Environ. Sci.* **2014**, *7*, 576–591.

85 Figueiredo, J.; Pereira, M.; Freitas, M.; Órfão, J. *Carbon* **1999**, *37*, 1379–1389.

86 Pimenta, M.; Dresselhaus, G.; Dresselhaus, M.; Cançado, L.; Jorio, A.; Saito, R. *Phys. Chem. Chem. Phys.* **2007**, *9*, 1276-1290.

Table Titles

Table 1. Catalytic Behaviors of Au-Pd Bimetallic Nanoparticles (Au/Pd = 1/1) Loaded on Various Supports for Aerobic Oxidation of HMF

Table 2. Effect of Loading Amount of Au-Pd Nanoparticles on Catalytic Behaviors of Au-Pd/CNT (Au/Pd = 1/1) Catalysts for Aerobic Oxidation of HMF

Table3. Relative Concentrations of Functional Groups over the Au-Pd/CNT (Au/Pd = 1/1) Catalysts with CNTs Pretreated by Different Methods

Table 4. Adsorption Amounts of HMF and Possible Intermediates (DFF and FFCA) from Aqueous Solutions onto CNTs Pretreated by Different Methods

Table 5. Effect of Modification by Model Organic Molecules on Catalytic Behavior of Au-Pd/Al_2O_3 (Au/Pd = 1/1) Catalyst for Aerobic Oxidation of HMF

Table 6. Catalytic Behaviors of Au-Pd/CNT Catalysts with Different Au/Pd Ratios as Well as Au/CNT and Pd/CNT for Aerobic Oxidation of HMF

Table 7. Rates of HMF, DFF, and FFCA Conversions at the Initial Reaction Stage over Au/CNT, Pd/CNT, and Au-Pd/CNT (Au/Pd = 1/1) Catalysts

Table 1. Catalytic Behaviors of Au-Pd Bimetallic Nanoparticles (Au/Pd = 1/1) Loaded on Various Supports for Aerobic Oxidation of HMF[a]

catalyst[b]	(Au + Pd) loading[c] (wt%)	Au/Pd[c] (molar ratio)	particle size (nm)	conv. (%)	Selectivity[d] (%)		
					DFF	FFCA	FDCA
Au-Pd/SiO_2	0.96	0.99	3.3	23	50	38	2.3
Au-Pd/Al_2O_3	0.99	0.99	2.4	34	45	43	2.9
Au-Pd/TiO_2	0.99	1.00	2.4	28	48	43	0
Au-Pd/ZrO_2	0.98	1.01	2.6	30	45	41	0
Au-Pd/CeO_2	0.95	1.01	2.6	32	48	43	0
Au-Pd/MgO	0.97	1.00	2.7	100	0	0.7	99
Au-Pd/HT	0.96	0.99	2.7	100	0	7.9	91
Au-Pd/CNF	0.96	0.99	2.4	59	30	50	15
Au-Pd/CNT	0.96	0.99	2.5	100	0	1.7	94
Au-Pd/CNT[e]	0.96	0.99	2.5	100	0	4.6	91
Au-Pd/GO	0.97	0.99	2.6	97	6.0	55	34

[a]Reaction conditions: HMF, 0.50 mmol ; HMF/(Au + Pd) (molar ratio), 100/1; H_2O, 20 mL; O_2, 0.5 MPa; temperature, 373 K; reaction time, 12 h. [b]HT, CNF, CNT, and GO denote hydrotalcite, carbon nanofiber, carbon nanotube, and graphene oxide, respectively; the CNT and CNF were pretreated by 5 wt% HCl at 323 K for 2 h. [c]Measured by ICP-MS. [d]DFF, FFCA, and FDCA denote 2,5-diformylfuran, 5-formyl-2-furancarboxylic acid, and 2,5-furandicarboxylic acid, respectively. [e]Reaction conditions: HMF, 3 mmol (0.15 M); HMF/(Au + Pd) (molar ratio), 100/1; H_2O, 20 mL; O_2, 0.5 MPa; temperature, 373 K; reaction time, 18 h.

Table 2. Effect of Loading Amount of Au-Pd Nanoparticles on Catalytic Behaviors of Au-Pd/CNT (Au/Pd = 1/1) Catalysts for Aerobic Oxidation of HMF[a]

entry No.	(Au + Pd) loading[b] (wt%)	Au/Pd[b] (molar ratio)	HMF conv. (%)	selectivity[c] (%)			FDCA yield (%)
				DFF	FFCA	FDCA	
1	0	-	0.90	0	0	0	0
2	0.095	1.01	59	29	54	16	9.7
3	0.20	1.00	83	18	48	32	27
4	0.48	0.99	98	3.7	31	63	62
5	0.67	0.99	100	0	6.1	92	92
6	0.96	0.99	100	0	1.7	94	94
7[d]	0.96	0.99	100	0	1.9	96	96

[a]Reaction conditions: HMF, 0.50 mmol; catalyst, 0.090 g; H_2O, 20 mL; O_2, 0.5 MPa; temperature, 373 K; reaction time, 12 h. [b]Measured by ICP-MS. [c]DFF, FFCA, and FDCA denote 2,5-diformylfuran, 5-formyl-2-furancarboxylic acid, and 2,5-furandicarboxylic acid, respectively. [d]Air, 1.0 MPa.

Table 3. Relative Concentrations of Functional Groups over the Au-Pd/CNT (Au/Pd = 1/1) Catalysts with CNTs Pretreated by Different Methods[a]

functional groups	normalized concentration of functional groups over CNTs with different pretreatments[b] (%)			
	5% HCl	30% HNO_3	68% HNO_3	30% H_2O_2
(a) CO_2 desorption peak				
carboxyl (~540 K)	19	50	100	27
anhydride (~650 K)	23	46	100	86
ester (750-830 K)	32	54	84	100
lactone (900-1010 K)	24	46	100	92
(b) CO desorption peak				
anhydride (~780 K)	34	60	100	82
phenol (~930 K)	74	58	35	100
carbonyl/quinone (1060-1150 K)	74	28	16	100

[a]Estimated from the desorbed CO and CO_2 peaks in TPD spectra. See Supporting Information Figure S2 for details. [b]The concentration of the strongest peak for each functional group among the four differently pretreated CNTs has been normalized to 100%.

Table 4. Adsorption Amounts of HMF and Possible Intermediates (DFF and FFCA) from Aqueous Solutions onto CNTs Pretreated by Different Methods

pretreatment	adsorption amount (μmol $g_{support}^{-1}$)			FDCA yield[b] (%)
	HMF	DFF	FFCA	
5 wt% HCl[a]	51	77	74	76
30 wt% HNO_3[a]	38	47	36	31
68 wt% HNO_3[a]	19	29	26	0
30 wt% H_2O_2[a]	68	78	76	95

[a]The adsorption was performed by addition of 0.10 g support into 10 mL aqueous solution containing 10 μmol adsorbate. [b]FDCA yield for the aerobic oxidation of HMF over the supported Au-Pd catalysts under the conditions in Figure 5.

Table 5. Effect of Modification by Model Organic Molecules on Catalytic Behavior of Au-Pd/Al_2O_3 (Au/Pd = 1/1) Catalyst for Aerobic Oxidation of HMF[a]

model molecules[b]	conv. (%)	selectivity[c] (%)			FDCA yield (%)
		DFF	FFCA	FDCA	
none	34	45	43	2.9	1.0
benzoic acid	29	50	48	1.7	0.5
phenol	32	40	52	7.8	2.5
quinone	63	23	33	42	26

[a]Reaction conditions: HMF, 0.50 mmol; HMF/(Au + Pd) (molar ratio), 100/1; H_2O, 20 mL; O_2, 0.5 MPa; temperature, 373 K; reaction time, 12 h. [b]The Au-Pd/Al_2O_3 (0.10 g) was added into an aqueous solution (5 mL) containing model molecules (1.0 mmol), and the suspension was stirred for 12 h at 303 K, followed by resting for another 12 h. After the adsorption, the catalyst was recovered by centrifugation and drying at 353 K, and then was used for catalytic reactions. [c]DFF, FFCA, and FDCA denote 2,5-diformylfuran, 5-formyl-2-furancarboxylic acid, and 2,5-furandicarboxylic acid, respectively.

Table 6. Catalytic Behaviors of Au-Pd/CNT Catalysts with Different Au/Pd Ratios as Well as Au/CNT and Pd/CNT for Aerobic Oxidation of HMF[a]

catalyst[b]	(Au + Pd) loading[c] (wt%)	Au/Pd[c] (molar ratio)	conv. (%)	selectivity[d] (%)			
				DFF	HMFCA	FFCA	FDCA
Au/CNT[e]	0.98	-	78	3.8	16	8.3	1.4
Au-Pd(4/1)/CNT	0.97	3.9/1.0	75	0	0	47	51
Au-Pd(7/3)/CNT	0.96	6.9/1.0	90	3.6	0	33	53
Au-Pd(1/1)/CNT	0.96	0.99/1.0	100	0	0	1.7	94
Au-Pd(3/7)/CNT	0.97	3.0/7.0	100	0	0	5.0	90
Au-Pd(1/4)/CNT	0.97	1.0/4.0	76	16	0	39	42
Pd/CNT	0.99	-	63	40	0	49	11

[a]Reaction conditions: HMF, 0.50 mmol; HMF/(Au + Pd) (molar ratio), 100/1; H_2O, 20 mL; O_2, 0.5 MPa; temperature, 373 K; reaction time, 12 h. [b]The number in the parenthesis denotes the Au/Pd molar ratio used for preparation; loading amount of (Au + Pd) expected, 1.0 wt%. [c]Measured by ICP-MS. [d]HMFCA denotes 5-hydroxymethyl-2-furancarboxylic acid. [e]Ring-opening and degradation products were formed.

Table 7. Rates of HMF, DFF, and FFCA Conversions at the Initial Reaction Stage over Au/CNT, Pd/CNT, and Au-Pd/CNT (Au/Pd = 1/1) Catalysts[a]

elementary reaction step[b]	rate[c] (μmol g_{cata}^{-1} s^{-1})		
	Au/CNT	Pd/CNT	Au-Pd/CNT
Step 1: oxidation of HMF to DFF	5.0	14	111
Step 1': oxidation of HMF to HMFCA	31	0	0
Step 2: oxidation of DFF	59	93	134
Step 3; oxidation of FFCA	0.34	41	75

[a] Reaction conditions: reactant, 0.50 mmol; reactant/(Au + Pd) (molar ratio), 200/1; H_2O, 20 mL; O_2, 0.5 MPa; temperature, 373 K. [b]See Scheme 1 for details. [c]Evaluated from Figure 7, Supporting Information Figures S7-S10.

Figure Captions

Figure 1. (a) TEM micrograph (dark field), (b) and (c) line-scan EDS analyses across two nanoparticles (red lines on the TEM micrograph, the mean particle sizes being ~4.0 and ~2.3 nm) for the Au-Pd/CNT (Au/Pd = 1/1) catalyst.

Figure 2. XPS spectra of (a) Au4f and (b) Pd3d in the Au-Pd/CNT (Au/Pd = 1/1) and Au/CNT or Pd/CNT catalysts.

Figure 3. Stability of the Au-Pd/MgO (a) and Au-Pd/HT (b) (Au/Pd = 1/1) catalysts during the recycling uses for the aerobic oxidation of HMF. Reaction conditions: HMF, 0.50 mmol; HMF/(Au + Pd) (molar ratio), 100/1; H_2O, 20 mL; O_2, 0.5 MPa; temperature, 373 K; reaction time, 12 h.

Figure 4. Stability of the Au-Pd/CNT (Au/Pd = 1/1) catalyst during the recycling uses for the aerobic oxidation of HMF. Reaction conditions: HMF, 0.50 mmol; HMF/(Au + Pd) (molar ratio), 100/1; H_2O, 20 mL; O_2, 0.5 MPa; temperature, 373 K; reaction time, 12 h.

Figure 5. Effect of the pretreatment of CNTs on catalytic behaviors of the Au-Pd/CNT (Au/Pd = 1/1) catalysts for the aerobic oxidation of HMF. Reaction conditions: HMF, 0.50 mmol; HMF/(Au + Pd) (molar ratio), 100/1; H_2O, 20 mL; O_2, 0.5 MPa; temperature, 373 K; reaction time, 10 h.

Figure 6. Time course for the conversion of HMF over the Au-Pd/CNT (Au/Pd = 1/1) catalyst. Reaction conditions: HMF, 0.50 mmol; HMF/(Au + Pd) (molar ratio), 100/1; H_2O, 20 mL; O_2, 0.5 MPa; temperature, 373 K.

Figure 7. Time course for the conversions of HMF over the Au/CNT catalyst. Reaction conditions: HMF, 0.50 mmol; HMF/Au (molar ratio), 200/1; H_2O, 20 mL; O_2, 0.5 MPa; temperature, 373 K. Others denote gluconic acid, glucuronic acid, succinic acid, glycolic acid, formic acid, carbon dioxide.

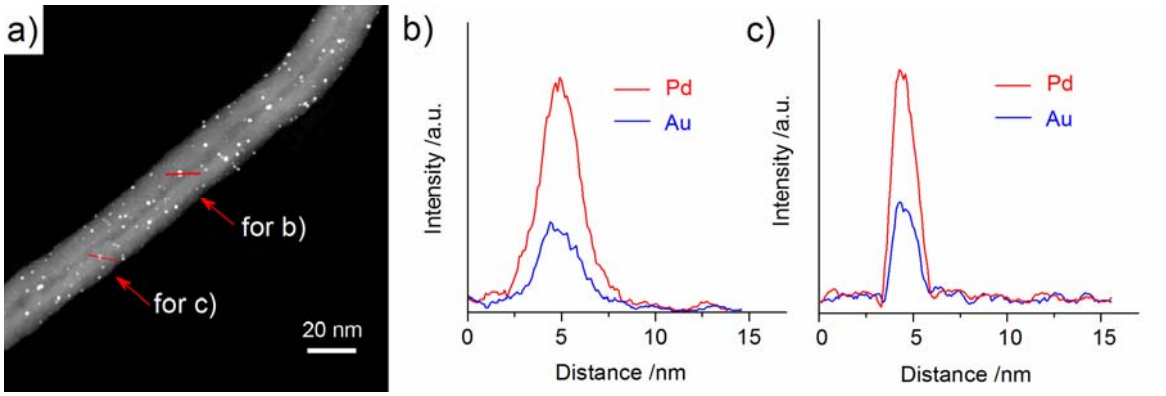

Figure 1. (a) TEM micrograph (dark field), (b) and (c) line-scan EDS analyses across two nanoparticles (red lines on the TEM micrograph, the mean particle sizes being ~4.0 and ~2.3 nm) for the Au-Pd/CNT (Au/Pd = 1/1) catalyst.

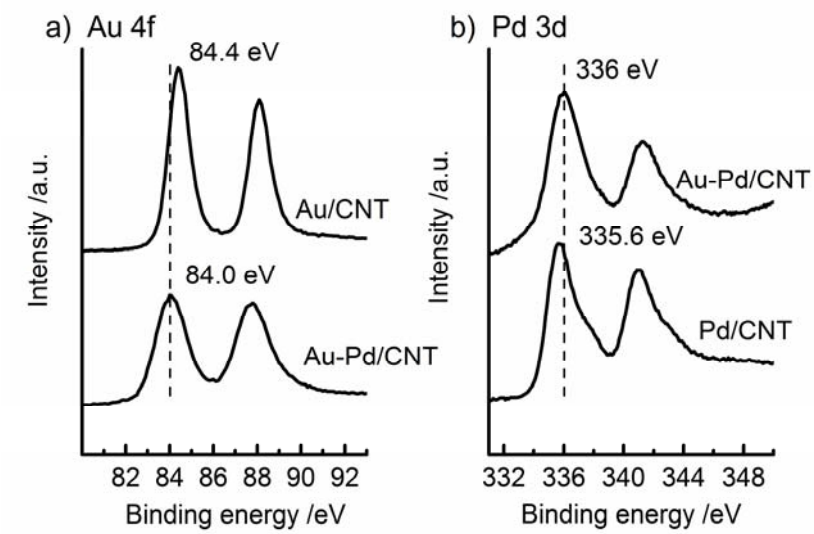

Figure 2. XPS spectra of (a) Au4f and (b) Pd3d in the Au-Pd/CNT (Au/Pd = 1/1) and Au/CNT or Pd/CNT catalysts.

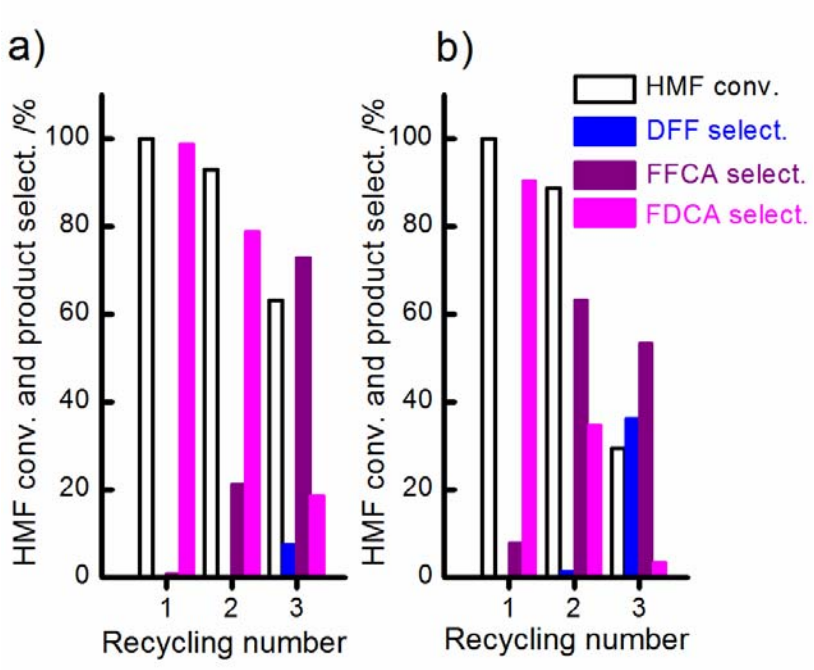

Figure 3. Stability of the Au-Pd/MgO (a) and Au-Pd/HT (b) (Au/Pd = 1/1) catalysts during the recycling uses for the aerobic oxidation of HMF. Reaction conditions: HMF, 0.50 mmol; HMF/(Au + Pd) (molar ratio), 100/1; H_2O, 20 mL; O_2, 0.5 MPa; temperature, 373 K; reaction time, 12 h.

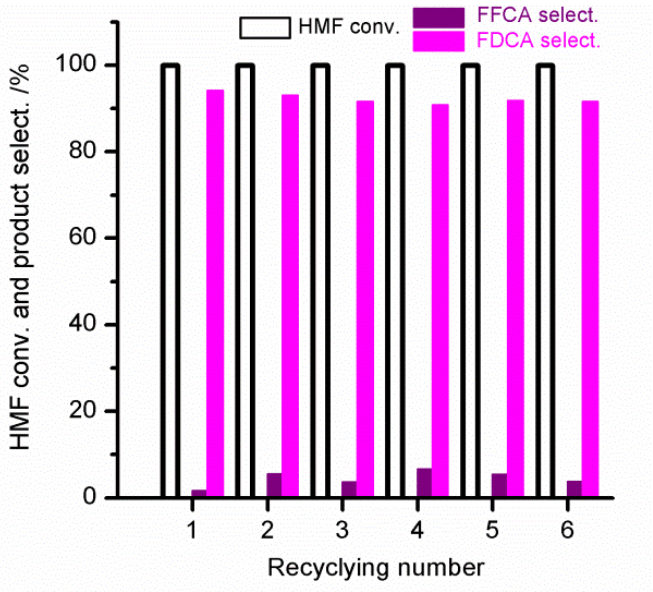

Figure 4. Stability of the Au-Pd/CNT (Au/Pd = 1/1) catalyst during the recycling uses for the aerobic oxidation of HMF. Reaction conditions: HMF, 0.50 mmol; HMF/(Au + Pd) (molar ratio), 100/1; H_2O, 20 mL; O_2, 0.5 MPa; temperature, 373 K; reaction time, 12 h.

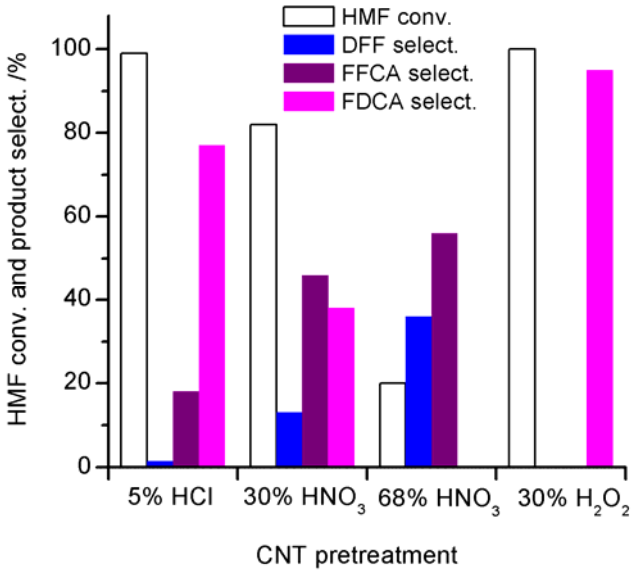

Figure 5. Effect of the pretreatment of CNTs on catalytic behaviors of the Au-Pd/CNT (Au/Pd = 1/1) catalysts for the aerobic oxidation of HMF. Reaction conditions: HMF, 0.50 mmol; HMF/(Au + Pd) (molar ratio), 100/1; H_2O, 20 mL; O_2, 0.5 MPa; temperature, 373 K; reaction time, 10 h.

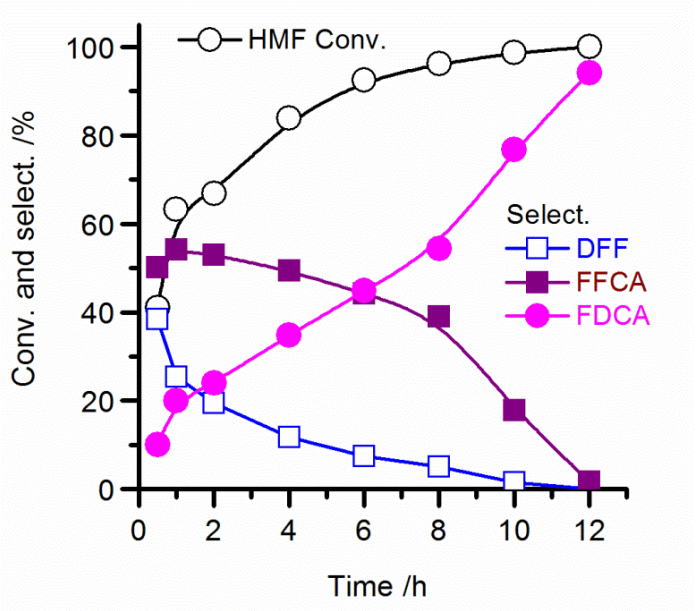

Figure 6. Time course for the conversion of HMF over the Au-Pd/CNT (Au/Pd = 1/1) catalyst. Reaction conditions: HMF, 0.50 mmol; HMF/(Au + Pd) (molar ratio), 100/1; H_2O, 20 mL; O_2, 0.5 MPa; temperature, 373 K.

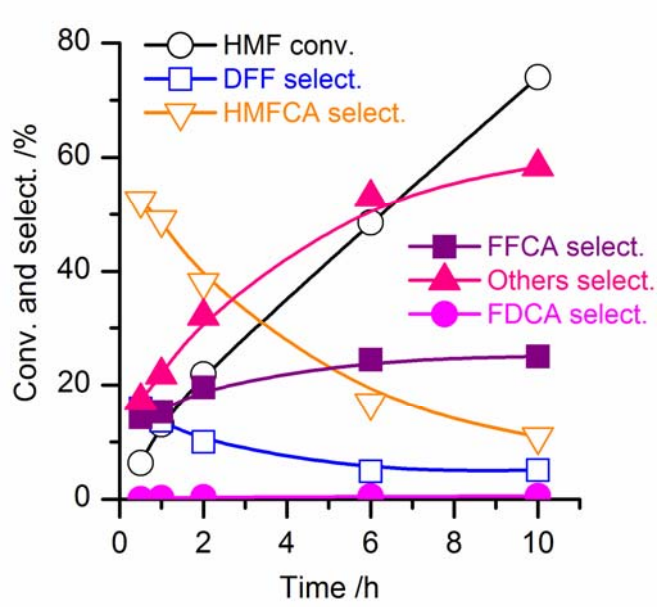

Figure 7. Time course for the conversions of HMF over the Au/CNT catalyst. Reaction conditions: HMF, 0.50 mmol; HMF/Au (molar ratio), 200/1; H_2O, 20 mL; O_2, 0.5 MPa; temperature, 373 K. Others denote gluconic acid, glucuronic acid, succinic acid, glycolic acid, formic acid, carbon dioxide.

Scheme

Scheme 1. Reaction Pathways for the Aerobic Oxidation of HMF, (a) Pd/CNT and Au-Pd/CNT Catalysts, (b) Au/CNT Catalyst.

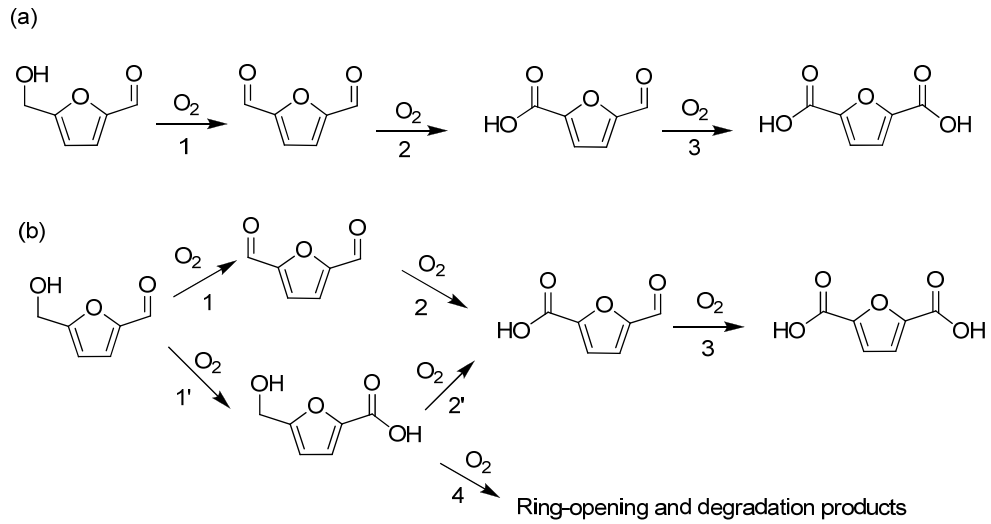

For Table of Contents Only

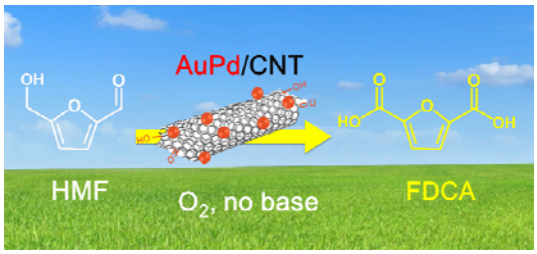

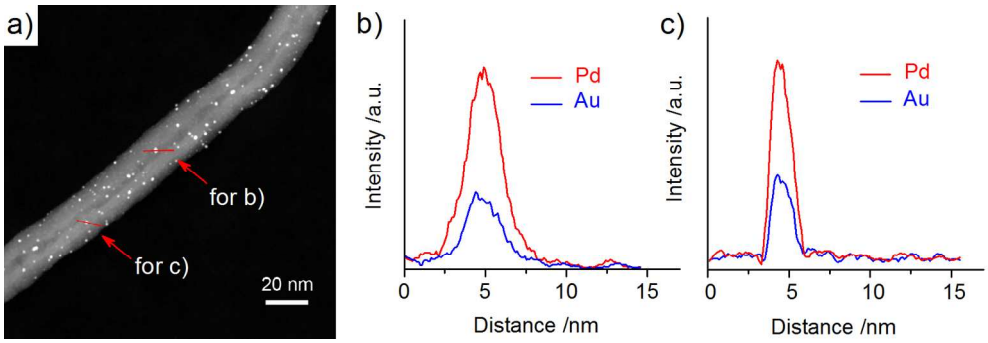

149x49mm (300 x 300 DPI)

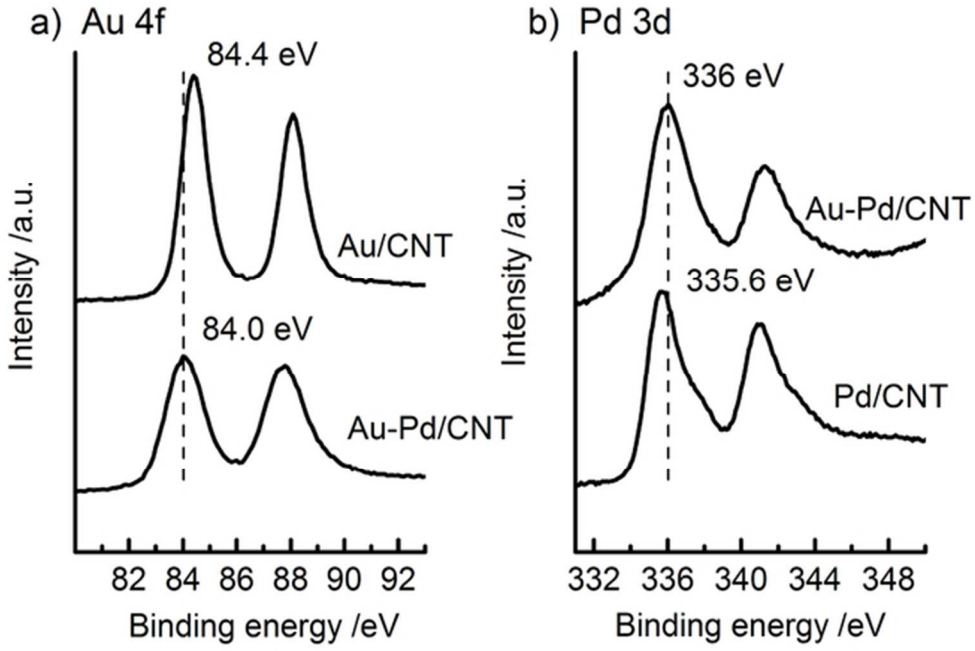

56x37mm (300 x 300 DPI)

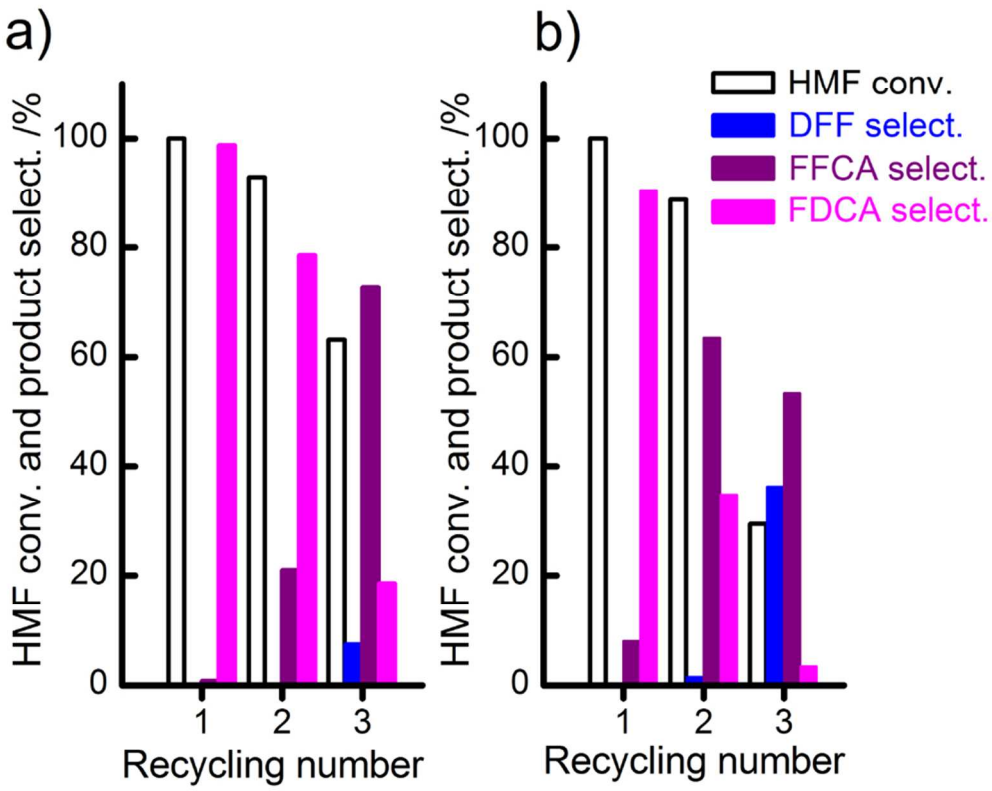

85x70mm (300 x 300 DPI)

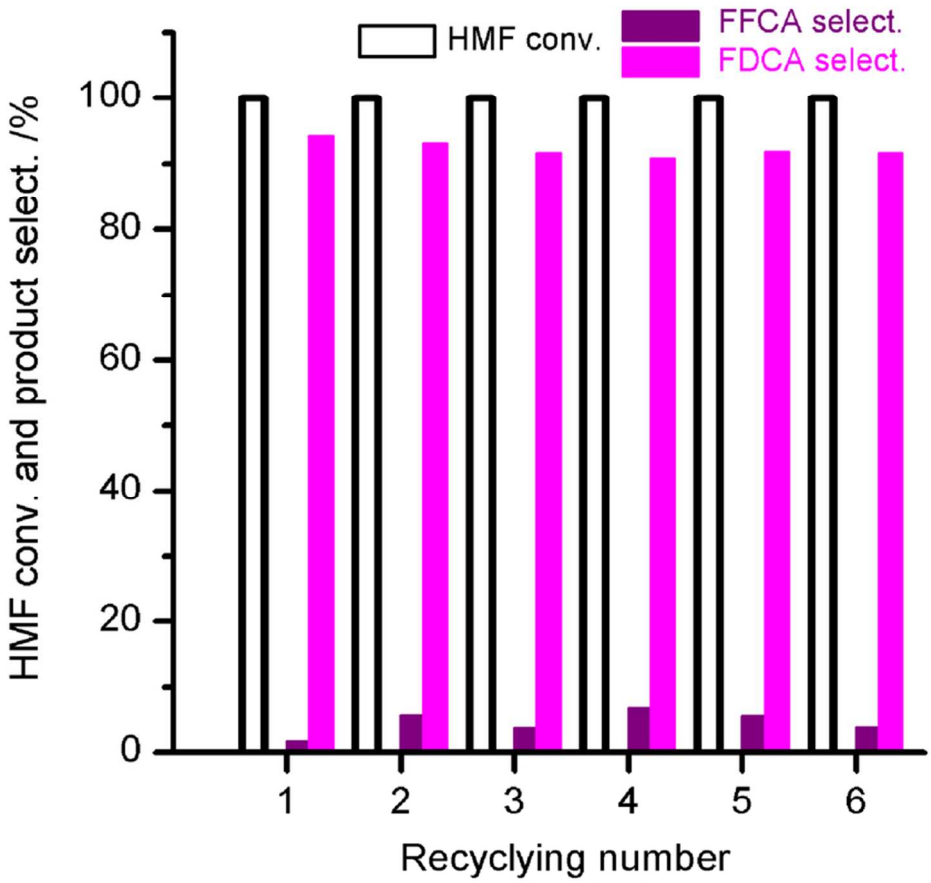

76x68mm (300 x 300 DPI)

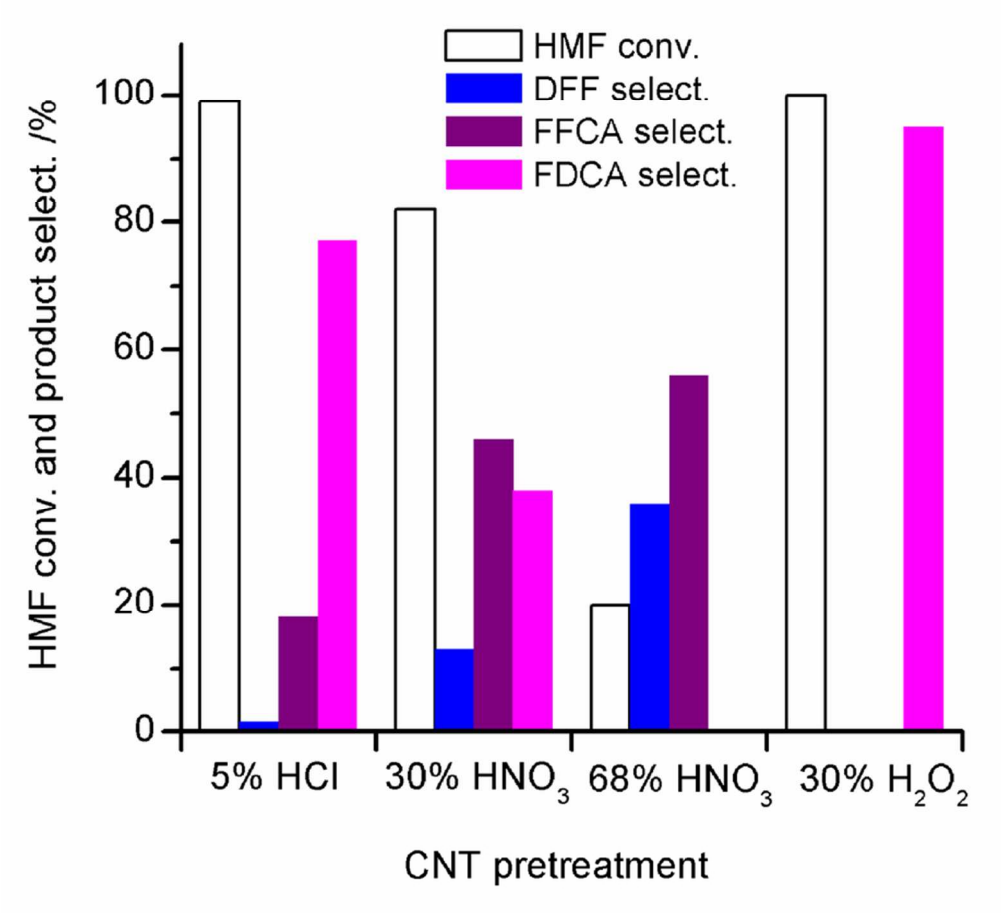

77x71mm (300 x 300 DPI)

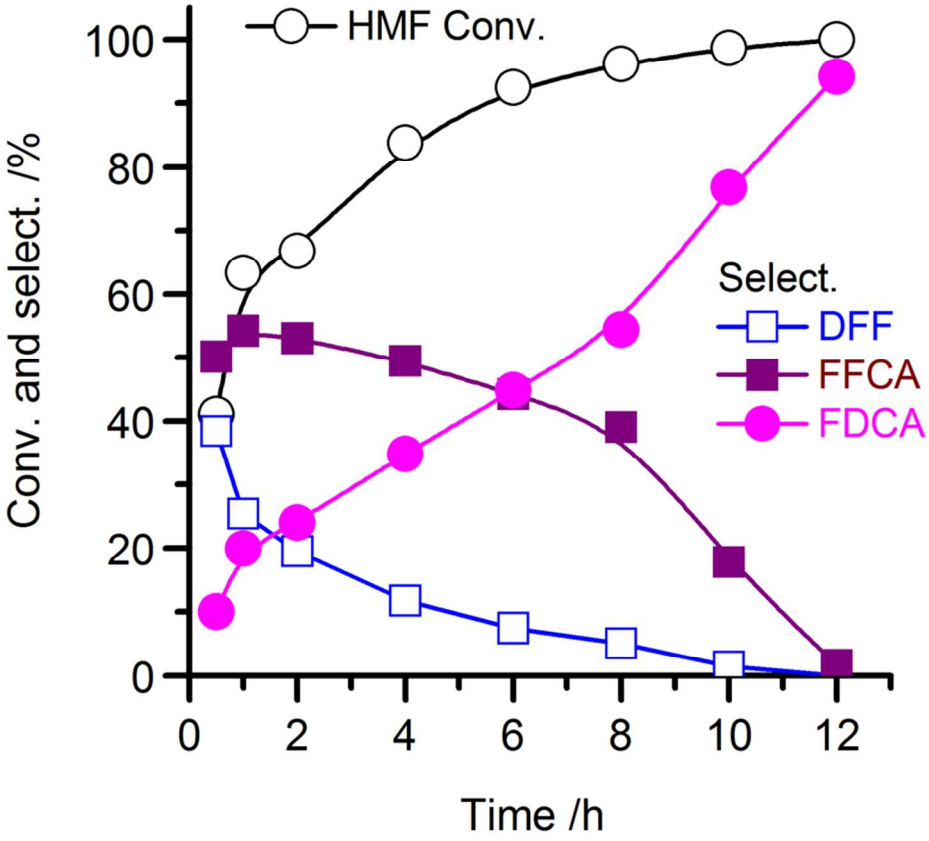

85x75mm (300 x 300 DPI)

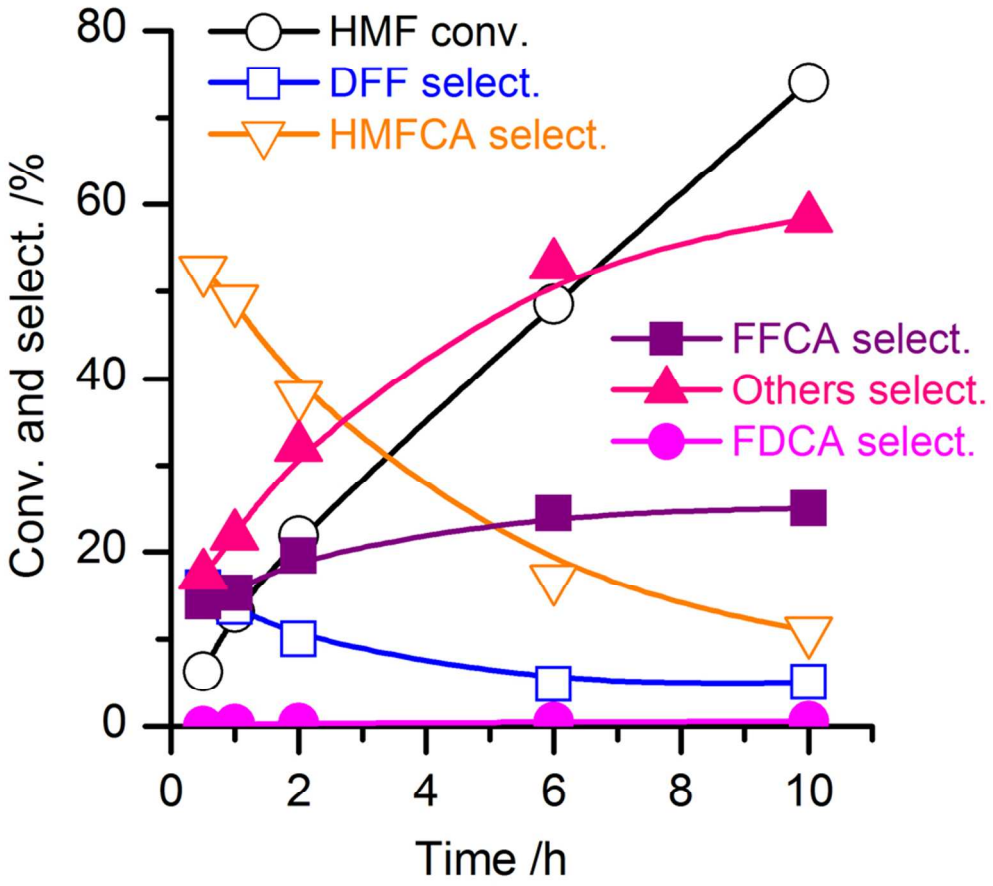

85x78mm (300 x 300 DPI)

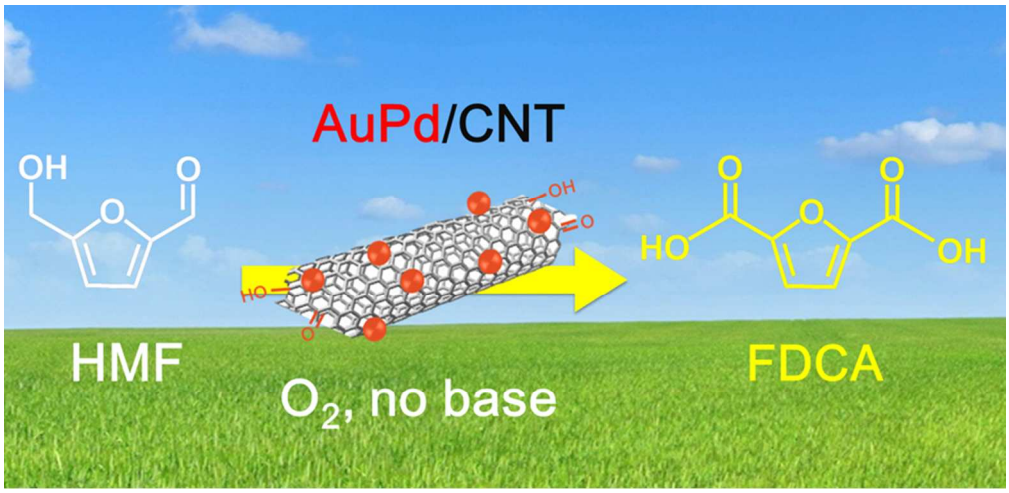

79x38mm (300 x 300 DPI)